

Electrochemical impedance and electrical resistance sensors for the evaluation of anticorrosive coating degradation

Zajec, Bojan; Bajt Leban, Mirjam; Lenart, Stanislav; Gavin, Kenneth; Legat, Andraž

DOI

[10.1515/corrrev-2016-0055](https://doi.org/10.1515/corrrev-2016-0055)

Publication date

2017

Document Version

Final published version

Published in

Corrosion Reviews

Citation (APA)

Zajec, B., Bajt Leban, M., Lenart, S., Gavin, K., & Legat, A. (2017). Electrochemical impedance and electrical resistance sensors for the evaluation of anticorrosive coating degradation. *Corrosion Reviews*, 35(2), 65-74. <https://doi.org/10.1515/corrrev-2016-0055>

Important note

To cite this publication, please use the final published version (if applicable).
Please check the document version above.

Copyright

Other than for strictly personal use, it is not permitted to download, forward or distribute the text or part of it, without the consent of the author(s) and/or copyright holder(s), unless the work is under an open content license such as Creative Commons.

Takedown policy

Please contact us and provide details if you believe this document breaches copyrights.
We will remove access to the work immediately and investigate your claim.

Original article

Bojan Zajec*, Mirjam Bajt Leban, Stanislav Lenart, Kenneth Gavin and Andraž Legat

Electrochemical impedance and electrical resistance sensors for the evaluation of anticorrosive coating degradation

DOI 10.1515/correv-2016-0055

Received October 22, 2016; accepted May 11, 2017; previously published online June 8, 2017

Abstract: Anticorrosive coatings are commonly used to protect metal structures from corrosion and thus assure constancy of the metal profile area, and consequently the mechanical stability of the metal structure. Due to environmental factors, corrosion of metal structures is inevitable and is considered during the design process; however, it is very difficult to predict the corrosion rate *a priori*, and the designer usually relies on empirical data to make an assessment. In an attempt to address this issue, various types of sensors that monitor the state of metallic coatings have been developed. In this study, the abilities of two systems, one based on electrochemical impedance and one using electrical resistance, developed by the authors to allow remote real-time monitoring of bridges are described. A laboratory study is presented in which three different sensor coating configurations were evaluated in three simulated environments: a salt spray chamber, a humid chamber, and an industrial chamber. The corrosion rates were monitored over a 9-month study period. Periodic measurements were made of the sensor output signals, and visual inspections (close-up photographs) were made to compare the visual and monitored response of the sensors. The sensitivity of the sensors is described, and the advantages and disadvantages concerning their deployment for field operations are discussed.

Keywords: anticorrosive coating; corrosion sensor; electrical resistance; monitoring; printed circuit board.

*Corresponding author: **Bojan Zajec**, Slovenian National Building and Civil Engineering Institute, Dimičeva 12, 1000 Ljubljana, Slovenia, e-mail: bojan.zajec@zag.si

Mirjam Bajt Leban, Stanislav Lenart and Andraž Legat: Slovenian National Building and Civil Engineering Institute, Dimičeva 12, 1000 Ljubljana, Slovenia

Kenneth Gavin: Technical University of Delft, Stevinweg 1, 2628 CN Delft, The Netherlands

1 Introduction

It is widely recognized that infrastructure managers over-rely on visual inspections as a means of managing risk on transport networks. A number of European Commission projects have been established to address this issue, including the SMARTRAIL project (SMARTRAIL), which aimed to provide advanced means of monitoring, assessment, and remediation of critical infrastructure on ageing European railway networks. Visual inspections require considerable manpower, pose a safety risk and delay potential with personnel on live tracks, and are often required on structures that are often not easily accessible. However, one of the biggest drawbacks with the approach is the human factor; the results of surveys are subjective and depend on the skills and experience of the inspector themselves. Recent major infrastructure failures (e.g. the collapse of the Malahide Viaduct in Ireland) have identified the loss of corporate knowledge leading to misleading visual assessments as a primary cause of catastrophic failure. Moreover, the periodic nature of visual assessments and the nature of many damage mechanisms, meaning that significant degradation is necessary before visual impact occurs, suggest that some form of continuous, remote monitoring will provide enhanced information of asset performance (Tam et al., 2007; Groysman, 2009). For the case of steel bridges, a viable solution is to remotely monitor corrosion progress on steel coated with anticorrosive paint at the structure site. Properly monitoring the structures for corrosion state and taking suitable measures at the appropriate time would result in enormous savings in terms of money, time, material, and energy. For this reason, suitable sensors are needed that convert the corrosion activity to some other, easily measureable quantity (Chen & Skerry, 1991; Davis et al., 2002; Dornbusch, 2008).

The existing sensors used for monitoring the degradation of organic coatings can be roughly divided into two groups based on their principle of operation, namely electrochemical and resistance types. The first group is most commonly used and consists of systems

that measure various electrical signals [most commonly electrochemical impedance spectroscopy (EIS), electrochemical noise (ECN), coupled multi-electrode arrays, etc.] between (embedded; Allahar et al., 2010) electrodes arranged in various configurations (Mansfeld, 1981; Gui & Brossia, 2008). These sensors are highly susceptible on the condition of the protective coating in terms of integrity (pinholes, defects, delamination, etc.), water absorption, and also the chemical composition of the environment. The group of resistance-based sensors measure the absolute resistance of the coated electrical conductor (substrate) based on the fact that this quantity increases with time due to the thinning caused by corrosion. Evidently, the conductor itself should be as thin as possible to allow the detection of minor damage. Electrical resistance (ER) sensors are less sensitive to coating degradation because they measure the corrosion that occurs as its consequence. However, the substrate thickness reduction (closely related to the corrosion rate) is usually exactly the quantity of interest for engineers and asset owners. Moreover, if a uniform rate of corrosion is assumed, then the relation between measured resistance and remaining thickness is unambiguous in contrast to electrochemical sensors where a model must be chosen to facilitate the interpretation (Mansfeld, 1993; Deflorian et al., 1999).

In this paper, sensors developed at the Slovenian National Building and Civil Engineering Institute for monitoring coatings on steel substrate are presented (Legat & Kuhar, 2008). A laboratory study was undertaken to evaluate the performance of two sensor types – one based on electrochemical impedance and the second based on resistivity. Three different configurations of organic coatings were applied to low-carbon steel, and the specimens were placed in three different corrosive environments with their response being measured over a 298-day monitoring period.

2 Materials and methods

2.1 Sensors

The sensors consist of a low-carbon steel substrate with applied coatings. The substrate was prepared in the form of electrodes fabricated using the printed-circuit-board (PCB) technique. For this purpose, a 300- μm low-carbon steel foil was laminated to a glass-fiber resin plate of 1 mm thickness and then photochemically etched to obtain the desired shape of the electrodes. Two types of electrode layouts were manufactured: (i) ER sensor (Legat, 2007;

Rosborg et al., 2011) and (ii) a so-called sensor kit consisting of 21 non-coupled, identically shaped electrodes (Figure 1). These electrodes allowed EIS and ECN measurements to be made. After the electrodes were manufactured, the investigated coatings were applied.

A PCB approach was essential for the production of ER sensors, as the substrate electrodes must be very thin to detect the small changes in the track thickness due to corrosion (Li et al., 2007). Moreover, the dimensions and shape of those tracks need to be within low tolerances for the proper functionality of the ER sensor. To enable comparison of the corrosion progress measured with ER sensors, the electrodes for EIS and ECN were also manufactured using the identical PCB technique.

The ER sensor developed is essentially a Wheatstone bridge with four identical long traces as legs. Two legs are coated with the coatings under investigation (Figure 2A), while the other two legs serve as a reference and are therefore protected against corrosion with another semi-transparent glass-fiber resin plate and glued with the transparent epoxy resin. The width of the traces is approximately 0.76 mm. The nominal surface area of one leg is 3.85 cm²; thus, the nominal exposed surface area is 7.7 cm². For the measurement, the Wheatstone bridge is powered with constant direct current of 50 mA, while the voltage

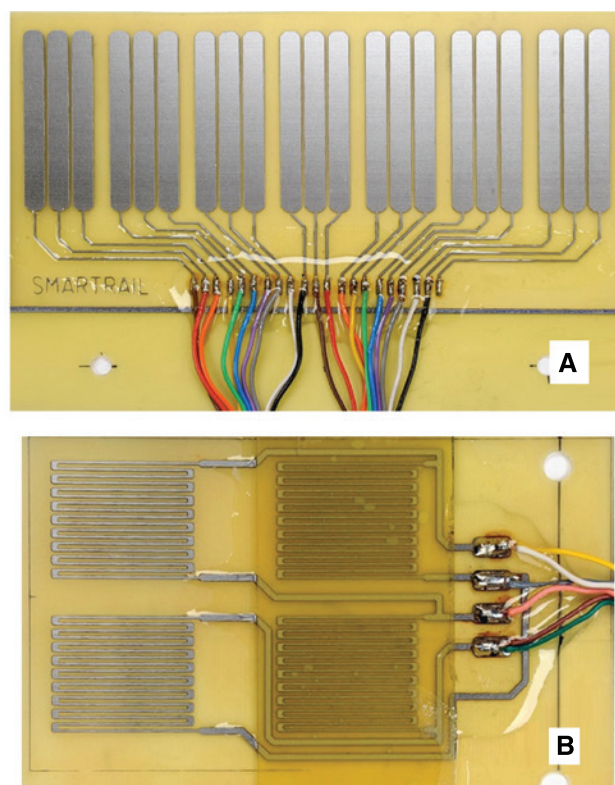


Figure 1: Sensor kit (A) and ER sensor (B) before coating.

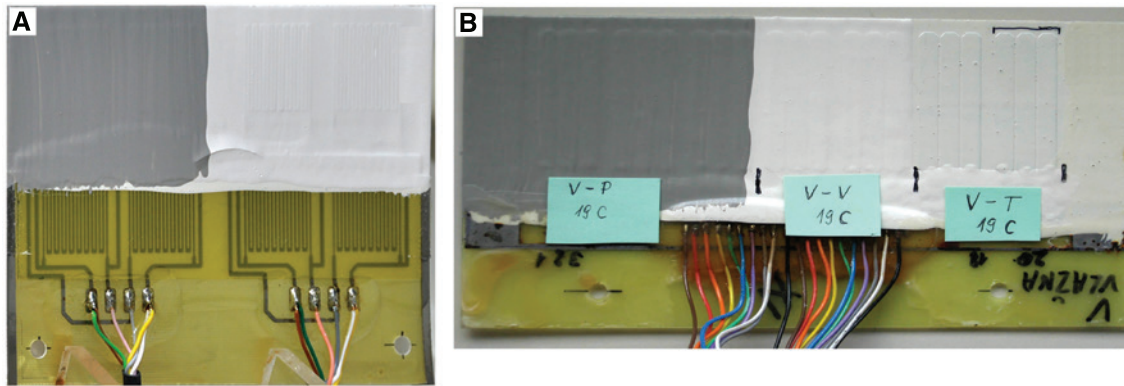


Figure 2: Sensors with coatings applied, ready for exposure: (A) ER sensors and (B) sensor kit.

drop U across the entire bridge is measured as well as the voltage difference ΔU between the midpoints (Legat et al., 2004). Assuming it is only the thickness of the exposed legs that is being uniformly reduced due to the corrosion, this reduction, Δd , can be expressed (Legat & Kuhar, 2008; Kranjc, 2016) as

$$\Delta d = d_0 \frac{2u}{1+u} \quad (1)$$

where d_0 is the initial trace thickness and $u = \Delta U/U$.

The sensor kit consisted of 21 identical electrodes, each $5.5 \text{ mm} \times 50 \text{ mm}$. In total, six electrodes were coated with only a primary coating (P); six electrodes were coated with primary and intermediate (P+I) coating; and the remaining nine were coated with the primary, intermediate, and top (P+I+T) coating (Figure 2B).

Both the ER sensors and sensor kits had the connection cables soldered to the dedicated connecting traces. The area around the cable connection was protected with a thick layer of transparent epoxy resin.

2.2 Coatings

The coatings investigated in this study are typical of those used for anticorrosion protection of steel railway bridges in Slovenia. The investigated coating system consists of three layers: a primer, an intermediate, and a top layer. The primer is a two-part high-build epoxy paint containing zinc phosphate; its commercial name is Epolor Special B. The intermediate coating is a two-part, high-build, high-solid, modified epoxy paint with low level of solvents. It exhibits good penetration properties and is commercially available as Epolor HB. The top coating is a two-part, high-build polyurethane paint with the commercial name Bukolit Emajl HB B. All three paints

are produced by Helios, Slovenia. The paints used for the primer and intermediate layers have good mechanical, thermal, and water (incl. salt water) resistance, and also good resistance against caustics and organic solvents. They have medium resistance against acids and poor resistance against ultraviolet light. The applied top coating displays excellence in all the abovementioned properties, with the exception of its resistance against acids, which is classified as medium. The selection of coatings is in agreement with the compatibility list provided by the producer in data sheets.

The thickness of the primary, intermediate, and top coating was 80, 140, and 60 μm , respectively. The lateral variation in the thickness was estimated to $\pm 20\%$. The coatings were applied manually with a brush. The primer was intentionally applied using rapid strokes in order to introduce air bubbles and consequently promote the formation of crater-like pinholes. In the pinhole, the coating is thinner and such sites are more susceptible to corrosion attack.

2.3 Exposure

The ER sensors and sensor kits with the three possible coating configurations (P, P+I, and P+I+T) were exposed to three different atmospheres in three dedicated environmental chambers. The environments considered included (i) a salt spray chamber (a salty water mist at 40°C , exposure according to the standard EN ISO 9227), (ii) a humid chamber (condensation of demineralized water at 40°C , EN ISO 6270), and (iii) an industrial SO_2 chamber (EN ISO 3231). The latter consists of cyclic exposure: 8 h of condensation of deionized (DI) water at 40°C along with a fraction of SO_2 gas in the atmosphere, followed by 16 h of drying at ambient conditions. The exposure was continuous and

only periodically interrupted for a short time to conduct measurements and visual inspection. The total time of exposure was 289 days.

2.4 Measurement procedures

After the ER sensors and sensor kits were taken from environmental chambers, they were first rinsed with DI water and dried. A visual inspection was then performed.

For EIS measurements, the sensor kit was immersed in an electrolyte comprising 0.1 M NaCl for sensors from the salt spray chamber and 0.1 M NaHCO₃ for sensors exposed in the humidity or industrial chambers. EIS measurements were carried out with Gamry 600 potentiostat (Gamry Instruments, USA) in a three-electrode configuration. The reference electrode was calomel electrode, while the counter-electrode was a graphite electrode. A single pre-selected trace under each coating (always the same trace) served as a working electrode. Impedance was measured at the open circuit potential E_{ocp} with 20 mV root mean square amplitude. A range of frequencies between 100 kHz and 10 MHz were investigated, with 10 points per decade. Prior to E_{ocp} measurement followed by EIS, the sensor kit

had been immersed for roughly 1 h. ECN measurements were not successful due to the several experimental and human errors, and will not be further elaborated here.

3 Results and discussion

3.1 Impedance

Analysis of the impedance measurements will focus mainly on the value $Z_{10\text{ mHz}}$ of the absolute impedance at the lowest measured frequency, 10 mHz (Bierwagen et al., 2003). As a rule of thumb, coatings with $Z_{10\text{ mHz}} > 100\text{ M}\Omega\text{ cm}^2$ are considered to provide an excellent anticorrosive protection, while $Z_{10\text{ mHz}}$ values $< 1\text{ M}\Omega\text{ cm}^2$ are characteristic of coatings with poor anticorrosive protection (O'Donoghue et al., 2003).

In Table 1, the evolution of $Z_{10\text{ mHz}}$ values vs. exposure time is presented for all three types of coatings in each of the three atmospheres. Despite certain outliers that might be due to experimental or human error, a general decreasing trend is evident. The degradation was most rapid for the primary coating in the salt spray chamber; hence, this

Table 1: Values of $Z_{10\text{ mHz}}$ in $\text{M}\Omega\text{ cm}^2$ vs. time for all three coating configurations.

Exposure (h)	Visual analysis	Salt spray chamber			Humid chamber			Industrial chamber		
		P	P+I	P+I+T	P	P+I	P+I+T	P	P+I	P+I+T
-120 ^a		1621.20	3276.00	31,510.50	2467.50	2835.00	2247.00	2656.50	2121.00	1585.50
48	At 72 h	36.87	191.84	144.17	631.79	135.45	110.67	31,605.00	211,260.00	158,823.00
96		<u>19.14^b</u>	124.53	73.44	21.11	65.73	65.28	19.64	39.66	20.69
168	X	0.79	94.87	35.09	11.45	39.26	38.35	20.34	32.68	24.27
192		2.64	77.29							
216		2.39								
240		2.23	75.12	26.89	9.51	28.85	33.93	10.31	24.48	17.04
360		0.16								
528		0.11								
600	X	0.06	34.25	19.45	<u>2.01</u>	10.04	15.30	<u>0.62</u>	16.18	15.24
864	X	0.03			1.87			0.17		
1200	X	0.023	22.932	14.900	1.080	<u>5.177</u>	<u>5.490</u>	0.086	12.443	8.562
1896		0.009	16.086	10.104	2.560	2.892	3.281	0.157	23.510	14.690
2568	X	0.007	0.036	0.035	0.915	2.541	1.617	0.172	27.909	17.409
3384	X	0.006	13.482	5.562	0.497	1.960	1.001	0.020	53.487	32.004
4128		0.012	15.330	6.777	0.122	1.190	0.058	0.006	55.230	39.312
5136		0.005	4.898	1.342	0.116	0.552	0.024	0.011	37.055	0.521
5808		0.005	4.816	1.911	0.101	0.620	0.134	0.010	42.010	0.918
6936		0.0026	5.734	1.739	0.131	0.481	0.030	0.006	42.010	2.531

The periods when visual analysis (incl. taking photos) was carried out are displayed with X sign. Underlined values indicate the first instance as the coating degradation was visually observed.

^a120 h before the start of the exposure.

^bFirst degradation noted at the visual inspection at 72 h into the exposure.

sensor has some extra data points. In the following, we will try to correlate (Mansfeld & Tsai, 1991) the obtained $Z_{10\text{ mHz}}$ values with the features on the images (detailed visual examination) of the EIS-measured trace (electrode). Times when the sensors were visually examined and photographed are also marked in Table 1, and the first occasion when coating degradation was noticed during visual inspection is marked with the underlined $Z_{10\text{ mHz}}$ value.

The primary coating layer on all three sensors had several crater-like pinholes. While they look like perfect candidates for corrosion attack, this was mostly not the case. A few less pronounced craters were present also at the P+I and P+I+T coating, as most of them were filled with P (and I) layer of the coating.

The primary coating from the salt spray chamber exhibited a very small rust spot only 72 h after the exposure, and at 168 h this spot was noticeably surrounded with a small rust stain. As time increased, corrosion products started to emanate from other locations and blistering started (Figure 3).

The primary coating from the humid chamber developed a blister at the bottom of the trace that was first noticed at the inspection 600 h after the exposure (Figure 4A). Between this and the preceding visual observation, the $Z_{10\text{ mHz}}$ decreased from 11.5 to 2.0 $\text{M}\Omega\text{ cm}^2$. The

situation remained apparently visually unchanged at least until the last inspection (3384 h) (Figure 4B). No corrosion products were observed.

A small and less pronounced blister at the bottom of the traces was observed also for P+I and P+I+T coating in the humid chamber at 1200 h for the first time as the $Z_{10\text{ mHz}}$ decreased to 5 $\text{M}\Omega\text{ cm}^2$ from values $>10\text{ M}\Omega\text{ cm}^2$. The blister size and visual appearance remained the same until the end of the measurement period; no rust stains appeared.

For the primary coating in the industrial chamber, a very small blister was noticed at the bottom of the trace 600 h after exposure (Figure 5). In the preceding period, the $Z_{10\text{ mHz}}$ decreased from 10.3 to 0.62 $\text{M}\Omega\text{ cm}^2$. At 864 h, small rust stains were noticed in close vicinity to three crater-like pinholes and the impedance decreased to 0.17 $\text{M}\Omega\text{ cm}^2$. Afterwards, this sensor further deteriorated and $Z_{10\text{ mHz}}$ reached the $\text{k}\Omega\text{ cm}^2$ range, which was similar to the primary coating exposed in the salt spray chamber.

The coatings of the remaining four sensors P+I and P+I+T from the salt and industrial chambers did not exhibit any visible degradation, which is well correlated to their final $Z_{10\text{ mHz}}$ values in the range of several $\text{M}\Omega\text{ cm}^2$ and even several tens of $\text{M}\Omega\text{ cm}^2$.

Judging from the decreasing trend of $Z_{10\text{ mHz}}$, it seems that the visual appearance of sensors other than those

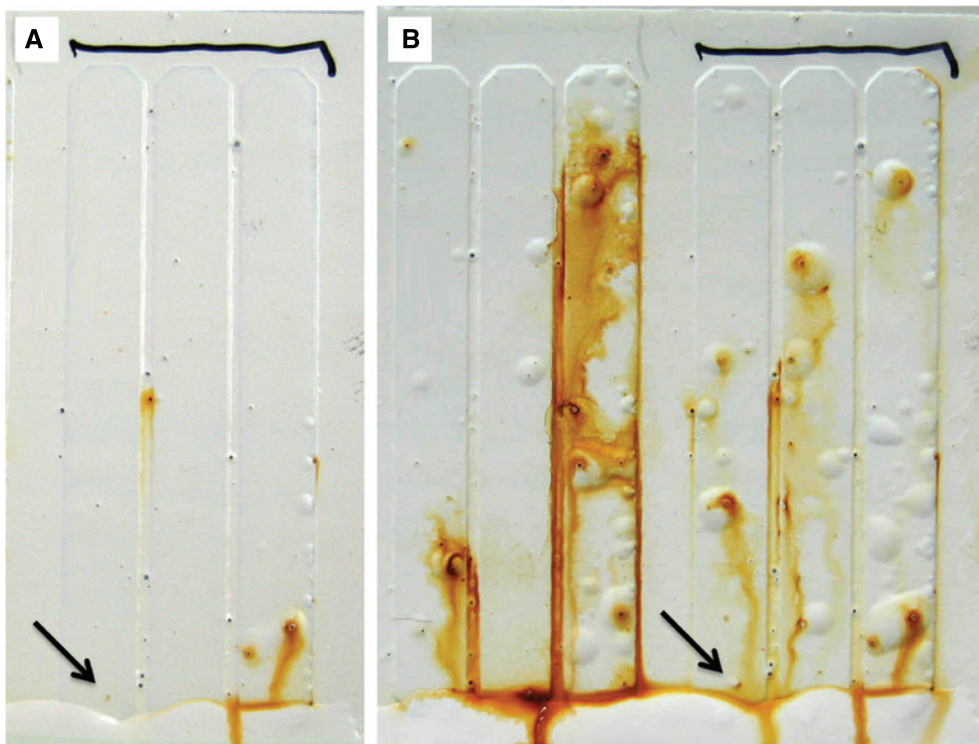


Figure 3: Primary coating exposed in the salt chamber after (A) 168 h and (B) 600 h. Arrows indicate the location where the first degradation on the EIS-inspected trace was noticed.

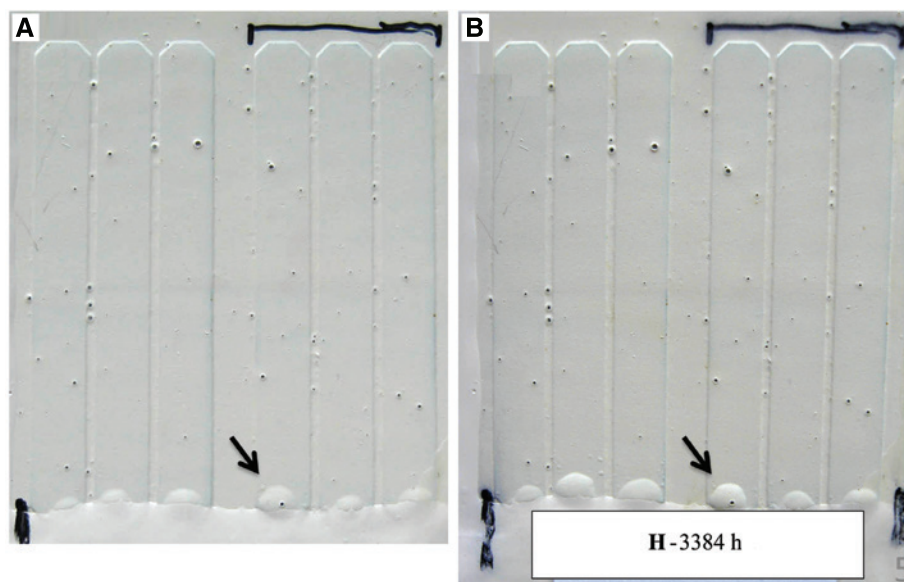


Figure 4: Primary coating exposed in the humid chamber after (A) 600 and (B) 3384 h. Arrows indicate the location where the first degradation on the EIS-inspected trace was noticed.

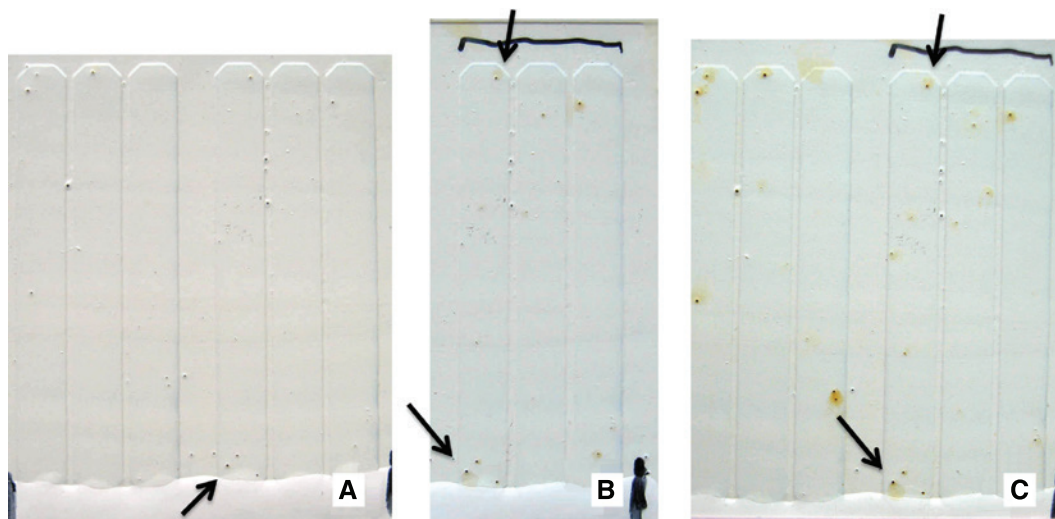


Figure 5: Primary coating exposed in the industrial chamber after (A) 600 h, (B) 864 h, and (C) 1200 h. Arrows indicate the location on the EIS-inspected trace where the degradation occurred – initially as a small blister and later as rust stains around crater-like pinholes.

with a primary coating does not provide a reliable correlation with the impedance measurements. Several sensors did not exhibit any visual degradation at all, or they had developed only a blister and no further damage occurred afterward, while the $Z_{10 \text{ mHz}}$ results indicated continuous degradation. During the experiment, it was realized that the glass-fiber resin plate was not perfectly impermeable (Pecht et al., 1999) and corrosion products could be observed at the backside of traces (electrodes) through the semi-transparent resin. Surprisingly, in certain cases, all traces with identical coatings had the

same oxidation pattern (Figure 6A). It was also found that the spots where the connection cable was soldered to the metal PCB trace were not sufficiently protected with the epoxy resin against the ingress of humidity and probably the electrolyte. Thus, the corrosion attacked the narrower connecting traces and, in certain cases, spread also to the wider traces covered with the examined layers of paints (Figure 6B). While this might provide a good explanation for the blisters described at the bottom of traces, no satisfactory correlation could be found; for example, all six P+I-covered traces from the humid chamber developed a

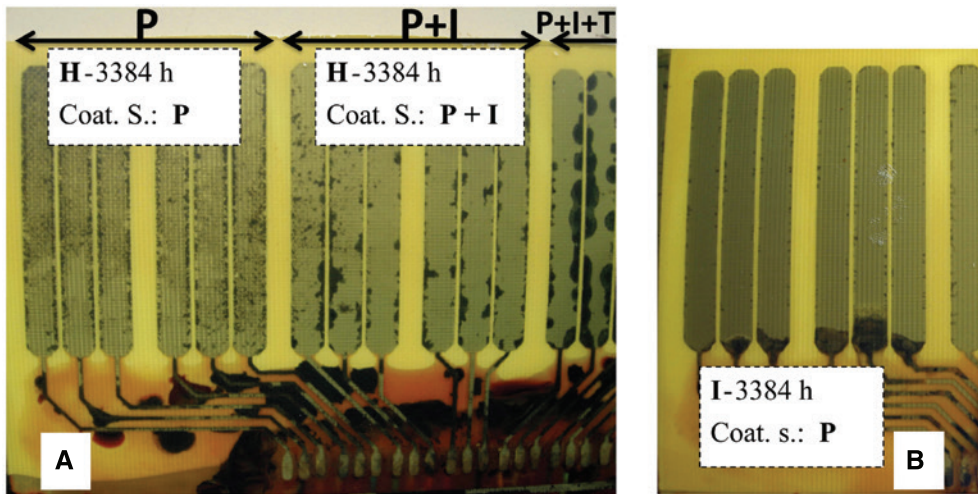


Figure 6: Oxidation of traces between the trace and glass-fiber resin plate as seen through the resin plate. (A) Oxidation patterns for the sensor kit exposed in the humid chamber after 3384 h and (B) oxidation attack through the narrower connection traces due to the bad protection by the epoxy resin.

blister at the bottom (Figure 4), while the corrosion products at their backsides (Figure 6A) were not concentrated at the bottom of traces.

From a certain point in time, these two unexpected processes dictated the impedance; hence, the results obtained after long exposure times do not necessarily reflect the condition of the coating only. One illustrative example is P+I coating exposed in the humid chamber. Its Bode plot (Figure 7) indicates a change in the corrosion mechanism between 3384 and 4128 h. Assuming that $Z_{10\text{mHz}}$ is a good approximation for the polarization resistance, the corrosion rate v_{corr} can be calculated as (Scully, 2000)

$$v_{\text{corr}} = \frac{M \cdot B}{n \cdot F \cdot \rho \cdot Z_{10\text{mHz}}} \quad (2)$$

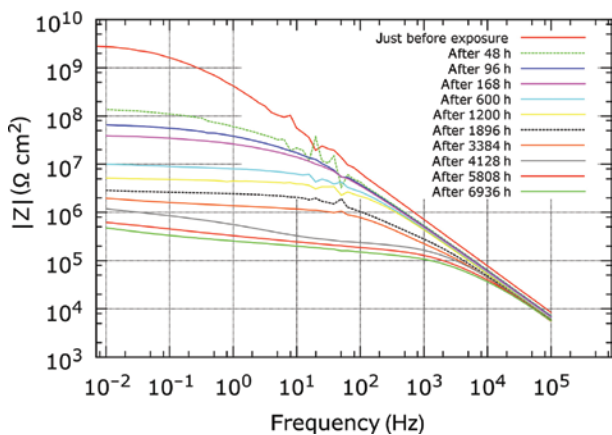
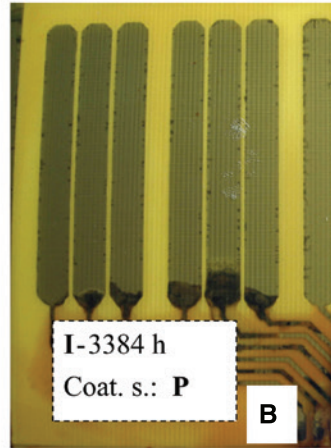


Figure 7: Bode plot of impedance modulus for P+I coating exposed in the humid chamber at different exposure times.



where M is molar mass (55.58 g/mol), B is Stern-Geary coefficient (26 mV as a common value; Papavinasam, 2008), n is valence of steel (2) and ρ its density (7.89 g/cm³), and F is Faraday constant. The corrosion rate vs. time for this sensor is shown in Figure 8. The corrosion rate initially increased linearly with time at a rate of 2.35 μm/year². Following the reading at 3384 h, this rate increased most likely due to the change in the corrosion mechanism or the onset of unwanted corrosion processes at the trace backside and/or soldering spots that are not related to coating degradation.

3.2 ER sensors

In contrast to the EIS measurement that reflects the corrosion state at that very moment, ER sensors reveal the

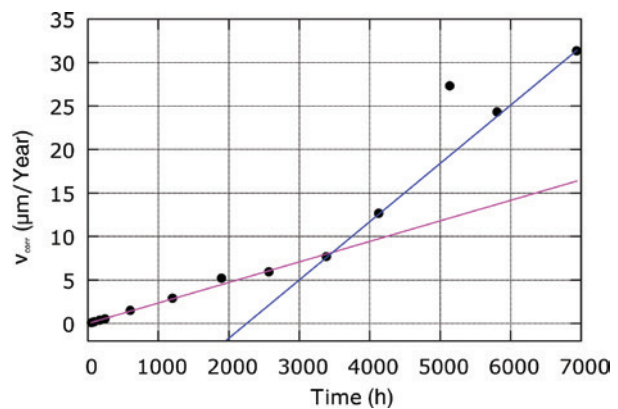


Figure 8: Corrosion rate vs. time based on EIS measurements for P+I coating exposed in the humid chamber.

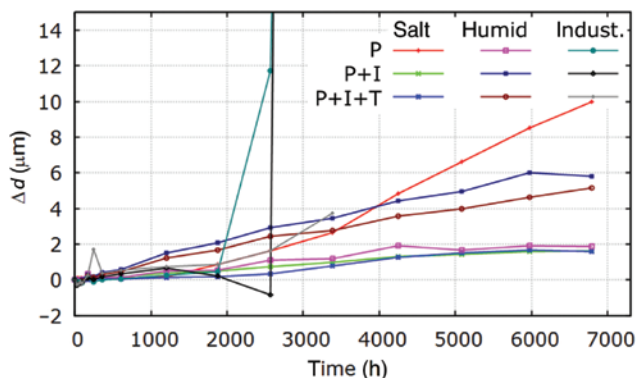


Figure 9: Trace thickness reduction Δd vs. time for all nine ER sensors.

entire time integral of the corrosion activity as the trace thickness reduction Δd is the main observable quantity. In Figure 9, the evolution of the thickness reduction is shown for all nine ER sensors. For the majority of sensors, Δd increased in a roughly linear fashion. Again, the primary coating from the salt spray chamber displayed the fastest deterioration, amounting to $\Delta d = 10 \mu\text{m}$ at the end of exposure, which corresponds to an average corrosion rate of $12.9 \mu\text{m}/\text{year}$. All ER sensors from the industrial chamber suffered a failure, most likely due to a localized corrosion that interrupted the measurement leg trace. This type of corrosion can be recognized by a sudden sharp increase of Δd that was measured at

3384 h, while at the next measurement (860 h later) they were already defective.

In general, the approach with ER sensors suffered from the same weaknesses as the sensors kits; that is, corrosion attack occurred through soldering spots and through the backside of the glass-fiber resin plate. However, in the present case, these processes had more serious impact on the reliability of corrosion detection under the investigated paint. The reason lies in the reference legs that must be left intact for the proper determination of the Δd value (Rosborg et al., 2011). Unfortunately, the traces of reference legs were closest to the soldering spots, and signs of corrosion attack there were evident already at 600 h, with the exception of ER sensors from the salt spray chamber. Later on, the corrosion products spread over large areas of reference leg traces and also measurement leg traces due to the permeable glass-fiber resin plate (Figure 10).

The deterioration of the reference leg traces was found to be minimal for sensors from the salt spray chamber, and for the primary coating ER sensor from this chamber its $\Delta d(t)$ was compared to $\Delta d_{\text{EIS}}(t)$ of the corresponding sensor kit (salt spray chamber, primary coating). The quantity $\Delta d_{\text{EIS}}(t)$ was obtained by numerical integration of $v_{\text{corr}}(t)$ given by Eq. (2); the values between two successive EIS measurements were obtained by linear interpolation of v_{corr} . The agreement between these two values is presented in Figure 11. From this figure, it follows that the ratio between EIS and ER measurements was approximately 3:1

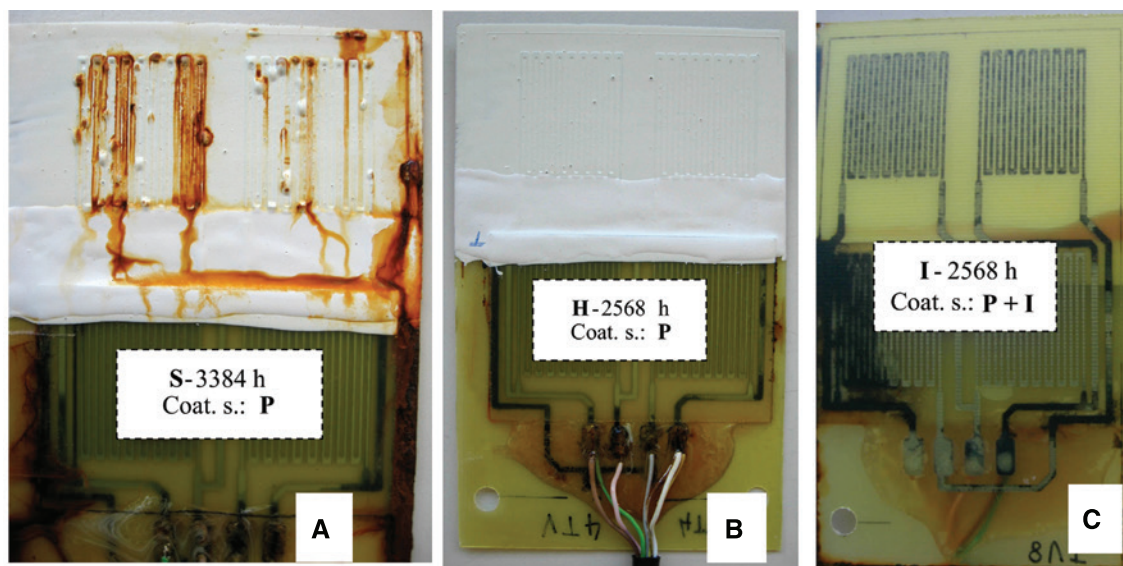


Figure 10: Unwanted oxidation of ER sensors. (A) Primary coating in the salt chamber after 3384 h of exposure; (B) primary coating in the humid chamber after 2568 h; and (C) P+I coating in the humid chamber after 2568 h of exposure (backside view). Oxidation of reference leg traces and spots where connection cable is soldered is visible in all three cases in various intensities. For case (C), the backside corrosion of measurement leg traces is also evident.

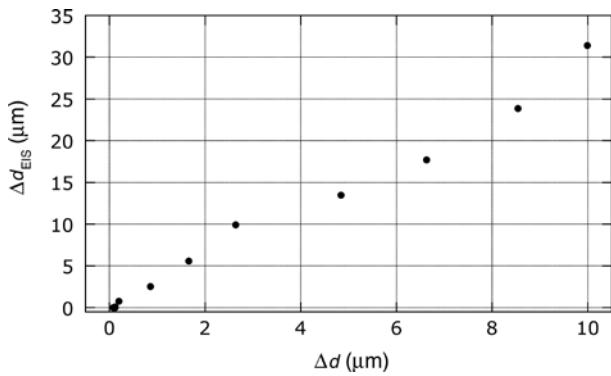


Figure 11: Comparison of trace thickness reduction obtained from ER sensor Δd to trace thickness reduction calculated from EIS measurements Δd_{EIS} for primary coating exposed in the salt chamber at identical times of exposure.

and the data points appear to be linearly correlated. Any further detailed comparison between EIS and ER results is not sensible, as the area of the ER sensors and particularly the area of the electrode used for the EIS are too small to be statistically representative due to the strong impact of localized corrosion attacks, be it through the coating layer or through the backside resin. An exception is perhaps the case of primary coating in the salt spray chamber that was heavily corroded from an early stage of exposure and thus approached to the state of general corrosion. As such, the comparison performed between the EIS and ER results has been presented only for this specimen (Figure 11). Values of Δd and Δd_{EIS} after the end of exposure (6900 h) given in Table 2 reveal only moderate agreement. This should not be looked upon as a shortcoming; it is more proper to use either Δd values or Δd_{EIS} values for ranking the coating quality, but not to mix and intercompare them.

Thickness reduction Δd obtained from the ER sensors is, in principle, more reliable for assessment of the substrate corrosion compared to Δd_{EIS} , as the former is in a simple relation to the measured resistance; hence, no models need to be assumed. Moreover, the ER sensors do not require immersion in the electrolyte for their operation, and thus avoid all ambiguities regarding the electrolyte

chemistry, immersion duration, and its impact on the results, as it is the case with electrochemical sensors. Significant localized corrosion attack is problematic for the interpretation of results obtained from both sensor types, as they both assume homogenous degradation and corrosion, and therefore report “averaged” values that can be significantly far from the actual state. This is particularly troublesome for EIS, as there is no good way to recognize from the measured results that small but influential localized corrosion is actually taking place (Philippe et al., 2003; Zhong et al., 2008), while for ER sensors it can be at least identified by a rapid increase in the resistance shortly before the measurement leg break, which means sensor failure. On the other hand, the sensitivity to the localized corrosion could be viewed also as beneficial, as such sensors provide some degree of warning even for localized degradation processes.

4 Conclusions

Quantitative assessment of the protection against corrosion provided by the three coating configurations was conducted using ER sensors and sensors based on EIS. The EIS sensor was found to be a highly sensitive technique, being able to detect early coating deterioration long before any visual signs appear and much earlier than a reliable signal was obtained using ER sensors. Due to several unknowns, such as equivalent circuit and homogeneity of the coating degradation, the EIS sensor should be viewed more like a semi-quantitative assessment. With ER sensors, the coating degradation can be assessed only indirectly, as they detect the thinning of the substrate due to the corrosion. Both sensor types are, in general, incapable of distinguishing localized corrosion and would report incorrect “averaged” values in the presence of intensive localized corrosion.

The current study revealed that the area of both types of sensors should be increased in order to get statistically representative results and take into the account the likelihood of localized corrosion. Careful manufacturing and material selection turned out to play a vital role as most of the tested coating configurations provided excellent corrosion protection. Special care must therefore be taken that the remaining non-coated areas are protected with an even more efficient material. Only this way can the observed corrosion processes be due to the corrosion attack through the coating.

When it comes to field application, which is the purpose of the research, the ER sensors are definitely

Table 2: Comparison of thickness reduction of coated steel obtained by EIS measurement (Δd_{EIS}) and ER sensors (Δd) at the end of exposure.

Chamber	Salt spray chamber			Humid chamber		
	P	P+I	P+I+C	P	P+I	P+I+C
Δd_{EIS} (μm)	34.39	0.73	0.80	1.07	0.21	2.67
Δd (μm)	9.99	1.63	1.60	1.88	5.80	5.16

more suitable, as the required electronics for powering and read-out is considerably simpler compared to the one for EIS-based sensors. Additionally, ER sensors inherently integrate the damage to the substrate done by the corrosion process during the entire exposure and thus avoid the need for frequent read-outs.

Acknowledgments: The work was funded by the European Union 7th Framework Programme under call SST.2011.5.2-6 Cost-effective improvement of rail transport infrastructure; grant agreement no. 285683.

References

- Allahar K, Su Q, Bierwagen G. Non-substrate EIS monitoring of organic coatings with embedded electrodes. *Prog Org Coat* 2010; 67: 180–187.
- Bierwagen G, Tallman D, Li J, He L, Jeffcoate C. EIS studies of coated metals in accelerated exposure. *Prog Org Coat* 2003; 46: 149–158.
- Chen C-T, Skerry B. Assessing the corrosion resistance of painted steel by AC impedance and electrochemical noise techniques. *Corrosion* 1991; 47: 598–611.
- Davis G, Krebs L, Dacres C. Coating evaluation and validation of accelerated test conditions using an in-situ corrosion sensor. *J Coat Technol* 2002; 74: 69–74.
- Deflorian F, Fedrizzi L, Rossi S, Bonora PL. Organic coating capacitance measurement by EIS: ideal and actual trends. *Electrochim Acta* 1999; 44: 4243–4249.
- Dornbusch M. The use of modern electrochemical methods in the development of corrosion protective coatings. *Prog Org Coat* 2008; 61: 240–244.
- Groysman A. Corrosion monitoring. *Corros Rev* 2009; 27: 205–343.
- Gui F, Brossia CS. Corrosion monitoring under coatings. In: Yang L, editor. *Techniques for corrosion monitoring*. Cambridge, England: Woodhead Publishing Limited, 2008: 436–447.
- Kranjc A. *Monitoring of copper corrosion in bentonite*. [Ljubljana, Slovenia]: Jožef Stefan International Postgraduate School, 2016.
- Legat A. Monitoring of steel corrosion in concrete by electrode arrays and electrical resistance probes. *Electrochim Acta* 2007; 52: 7590–7598.
- Legat A, Kuhar V. Sensor, device and procedure for determination of corrosion speed of metal reinforcement in reinforced concrete structures. Patent SI 22559 A. Slovenian Intellectual Property Office, 2008.
- Legat A, Leban M, Bajt Ž. Corrosion processes of steel in concrete characterized by means of electrochemical noise. *Electrochim Acta* 2004; 49: 2741–2751.
- Li S, Kim Y-G, Jung S, Song H-S, Lee S-M. Application of steel thin film electrical resistance sensor for in situ corrosion monitoring. *Sens Actuators B Chem* 2007; 120: 368–377.
- Mansfeld F. Evaluation of electrochemical techniques for monitoring of atmospheric corrosion phenomena. *Electrochemical Corrosion Testing*. ASTM International, 1981.
- Mansfeld F. Models for the impedance behavior of protective coatings and cases of localized corrosion. *Electrochim Acta* 1993; 38: 1891–1897.
- Mansfeld F, Tsai C. Determination of coating deterioration with EIS: I. Basic relationships. *Corrosion* 1991; 47: 958–963.
- O'Donoghue M, Garrett R, Datta V, Roberts P, Aben T. Electrochemical impedance spectroscopy: testing coatings for rapid immersion service. *Mater Perform* 2003; 42: 36–41.
- Papavinasam S. Electrochemical polarization techniques for corrosion monitoring. In: Yang L, editor. *Techniques for corrosion monitoring*. Cambridge, England: Woodhead Publishing Limited, 2008: 49–85.
- Pecht MG, Ardebili H, Shukla AA, Hagge JK, Jennings D. Moisture ingress into organic laminates. *IEEE Trans Compon Packag Technol* 1999; 22: 104–110.
- Philippe L, Walter G, Lyon S. Investigating localized degradation of organic coatings comparison of electrochemical impedance spectroscopy with local electrochemical impedance spectroscopy. *J Electrochem Soc* 2003; 150: B111–B119.
- Rosborg B, Kranjc A, Kuhar V, Legat A. Corrosion rate of pure copper in an oxic bentonite/saline groundwater environment. *Corros Eng Sci Technol* 2011; 46: 148–152.
- Scully JR. Polarization resistance method for determination of instantaneous corrosion rates. *Corrosion* 2000; 56: 199–218.
- SMARTRAIL. Smartrail project website [Internet]. Available from: <http://smartrail.fehrl.org>. Accessed 16 February, 2017.
- Tam H, Lee T, Ho S, Haber T, Graver T, Méndez A. Utilization of fiber optic Bragg Grating sensing systems for health monitoring in railway applications. *Struct Health Monit* 2007; 2: 1824–1831.
- Zhong C, Tang X, Cheng Y. Corrosion of steel under the defected coating studied by localized electrochemical impedance spectroscopy. *Electrochim Acta* 2008; 53: 4740–4747.